Journal of Magnetics 6(2), 53-56 (2001)

Thickness-Driven Spin Reorientation Transition in Co/Pd(111) : *In Situ* SMOKE Three-Dimensional Vector Magnetometry

Jeong-Won Lee[1], Sang-Koog Kim[1], Jonggeol Kim[1], Jong-Ryul Jeong[1], Jae-Seok Ahn[2] and Sung-Chul Shin[1]

[1]Department of Physics and Center for Nanospinics of Spintronic Materials, Korea Advanced Institute of Science and Technology, Taejon 305-701, Korea
[2]Department of Physics, University of Seoul, Seoul 130-020, Korea

(Received 15 September 2000)

We have developed a three-axis configurational *in situ* SMOKE apparatus by which three-dimensional vector magnetization reversal processes are studied for ultrathin Co films grown on a Pd (111) single crystal in the thickness range of spin reorientation transition. This study provides a better understanding of magnetization reversal motions with the knowledge of three components of the magnetization vector at the transition of an easy axis of magnetization from the film normal at 5 ML Co to in-plane at 6 ML Co (ML denotes monolayer). For a 5.25 ML Co, it was observed that a slightly canted magnetization vector from the film normal rotated in the film plane under an applied field direction parallel to the film normal.

1. Introduction

Understanding of magnetization orientations in zero or constant fields and/or magnetization reversal motion remains fundamental, so that investigation of three dimensional (3D) full magnetization vector is of great importance. The spin orientations in different domains or layers of magnetic thin films are closely associated with magnetic properties such as spin reorientation transition (SRT), giant magnetoresistance (GMR), and tunneling magnetoresistance (TMR), which are very interesting phenomena technologically applicable to very recent high-density information storage. Especially, SRT behavior has been important in ultrathin film magnetism because magnetic films having strong perpendicular magnetic anisotropy (PMA) are promising candidates for ultrahigh-density recording media.

Ultrathin Co films exhibit an enhanced PMA for thicknesses of a few monolayers [1, 2]. The PMA is sufficient to overcome demagnetizing energy of thin films and makes the spontaneous magnetization direction out-of-plane as the thickness decreases. In very recent work on SRT [3], anisotropy space of the first order (K_1) and second order anisotropy (K_2) constants is introduced in the framework of the anisotropy free energy in order to better understand magnetization switching behavior as a function of film thickness. This concept has predicted a metastable phase of coexistence of the in-plane and out-of-plane magnetization phases as well as a canted phase, which are dependent on the relative strength of K_1 and K_2. The work motivates us to develop a 3-configurational *in situ* surface magneto-optical Kerr effect (SMOKE) system to investigate 3D full vectorial magnetization and the magnetization reversal processes, especially in the thickness range of the spin reorientation transition of ultrathin films.

SMOKE is a premier technique for ultrathin magnetic film study because it has monolayer sensitivity and can be used *in situ* under ultrahigh vacuum (UHV) [4]. It has been widely utilized for investigation of magnetic properties such as magnetic anisotropy [5], magnetic phase transition [6], and SRT [7-9]. In our work, we choose Co films grown on a Pd(111) single crystal as a prototype. The vector nature of the magnetization reversal process is clearly identified for 5.0~6.0 ML Co films, where SRT occurs from out-of-plane to in-plane.

2. Experiments

The experiments were carried out in an ultrahigh vacuum chamber with a base pressure of 5×10^{-11} Torr, which was especially designed to permit 3-axis configurational *in situ* SMOKE measurements and deposition at the same position without sample transportation. Co films were grown on a single crystal Pd(111) substrate by e-beam evaporation with a deposition rate of 0.8 Å/min at room temperature. The Pd(111) substrate was cleaned by several cycles of sputtering with 1 keV Ar^+ ions followed by annealing at 900 K. Well-formed terrace structure of the Pd(111) surface was confirmed by STM study. Details of the SMOKE measurement system were described elsewhere [10].

To investigate 3D vectorial magnetization reversals of

ultrathin Co films in the thickness range where SRT occurs, we measured *in situ* Kerr rotation and ellipticity with an accuracy down to 0.001° through phase-sensitive detection using a precise photoelastic-modulator and crystal polarizers with extinction ratio of better than 10^{-5}. The sample stage could be rotated ± 60° in the film plane with a precision manipulator, allowing various measurement geometries at different scattering planes. To obtain SMOKE data needed for a complete analysis of 3D vectorial magnetization during magnetization reversals, SMOKE signals were taken using 3 configurations as depicted in Fig. 1: (1) two polar configurations in the *yz* and *xz* scattering planes with a magnetic field applied along the film normal; (2) longitudinal configuration in the *yz* scattering plane with an applied field parallel to the *y*-axis. These three configurational measurements are sufficient to obtain SMOKE data needed for 3D vectorial determination of the magnetization directions during magnetization reversal.

3. Description of 3D Vector Magnetometry using SMOKE

Very recently, we reported a magnetization reversal process for a Co thin film represented by 3D magnetization vector motion as a function of applied magnetic field using simplified analytic expressions for MOKE in a magnetic film where the ultrathin film has an arbitrary magnetization orientation and the probing light is obliquely incident to the film plane [11, 12]. When the scattering plane is located in the *yz* plane, complex Kerr effects for the *p*- and *s*-waves in the ultrathin limit, $\Theta^p(M_y, M_z)$ and $\Theta^s(M_y, M_z)$, are given as follows:

$$\Theta^p(M_y, M_z)=\frac{\cos\theta_0}{\cos(\theta_0+\theta_2)}\left(M_y\frac{\sin^2\theta_1}{\sin\theta_2}+M_z\cos\theta_2\right)\Theta_n, \tag{1-a}$$

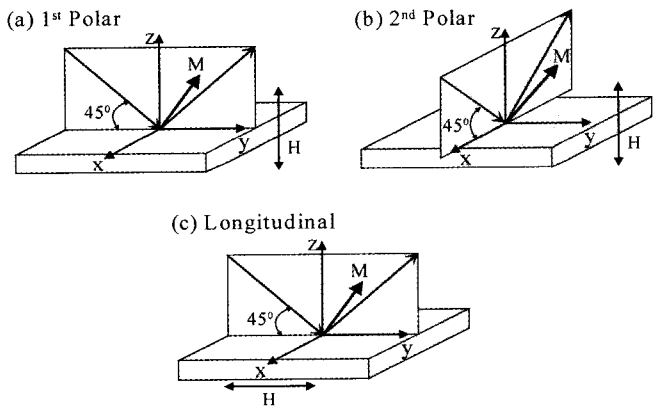

Fig. 1. The coordinate systems of three-axis configurations of SMOKE measurements: Polar Kerr measurements in the *yz* (a) and *xz* (b) scattering planes where the magnetic field is applied along the film normal; and longitudinal measurement in the *yz* (c) scattering plane where the magnetic field is parallel to the *y*-axis.

$$\Theta^s(M_y, M_z)=\frac{\cos\theta_0}{\cos(\theta_0-\theta_2)}\left(M_y\frac{\sin^2\theta_1}{\sin\theta_2}-M_z\cos\theta_2\right)\Theta_n, \tag{1-b}$$

where θ_0, θ_1, θ_2, Θ_n are the incident angle, complex refractive angles of the magnetic thin film and the nonmagnetic substrate, and the complex polar Kerr angle for normal incidence in the ultrathin film limit, respectively. Here, the incident angle is $\theta_0 = 45°$. M_y and M_z are the direction cosines of the magnetization vector in the *y*- and *z*-directions, respectively. In the case of *xz* scattering plane, M_y can be replaced by M_x. In general, θ_1, θ_2, and Θ_n in Eqs. (1) are sensitively dependent on the thickness and optical properties of a thin film; *in situ* determination of these values for a growing film is very difficult or at least requires another technique such as *in situ* ellipsometry for obtaining the exact values for the growing films. However, it is not necessary to directly measure those values for our vectorial analysis of magnetization orientations if the saturation values of Kerr angles for each growing film can be obtained as described below. All the components, M_x, M_y, and M_z can be determined as follows:

$$M_{x,y}=\frac{\Theta_P^s\Theta^p(M_{x,y}, M_z)-\Theta_P^p\Theta^s(M_{x,y}, M_z)}{\Theta_L^p\Theta_P^s-\Theta_P^p\Theta_L^s} \tag{2-a}$$

$$M_z=\frac{\Theta_L^s\Theta^p(M_{x,y}, M_z)-\Theta_L^p\Theta^s(M_{x,y}, M_z)}{\Theta_P^p\Theta_L^s-\Theta_L^p\Theta_P^s} \tag{2-b}$$

where, Θ_J^i denotes the saturation values of measured complex Kerr angles for the *i*-polarization wave (*i* = *s*- and *p*-waves) in *J*-measurement configuration. Therefore, one can determine all the components of magnetization vector ***M*** during the reversal process using only Eqs. (2).

4. Results and Discussion

Fig. 2 shows the evolution of polar and longitudinal SMOKE hysteresis loops with Co film thickness grown on a Pd(111) single crystal. For 1 ML Co, no hysteresis loop appears in either geometry. This can be ascribed to the loss of ferromagnetism, consistent with the Co/Au(111) case [13], where initial ferromagnetic order appears at 1.5 ML Co. Onset of appearance of Kerr rotation and coercivity occurs at 1.5 ML Co. Hysteresis loops and coercivities start to appear from 4 ML Co in longitudinal geometry. This is because the longitudinal coercivities of those thicknesses exceed the maximum field of 2 kOe available in our system in the range 1 ML < t_{Co} < 4 ML, as evident from the trend of the longitudinal coercivity with t_{Co}. Generally, the longitudinal coercivities below 4 ML Co are much larger than polar ones and drastically decrease with the small increase of Co coverage at the transition of magnetization orientation from perpendicular to in-plane. In the thickness range 2 ML ~ 4.5 ML, the coercivities of the polar loops are about

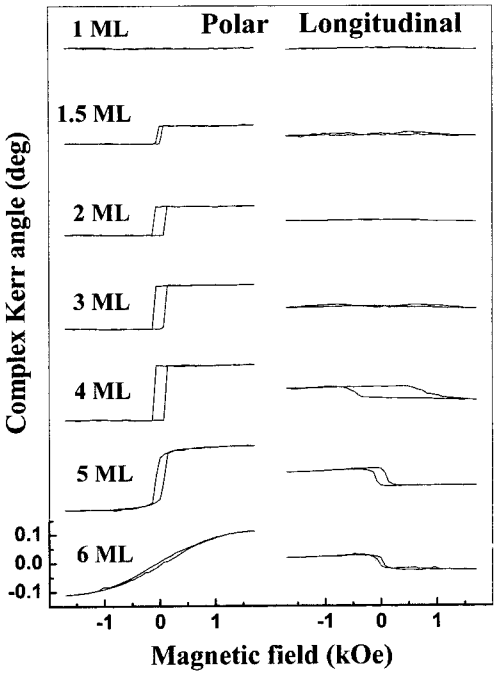

Fig. 2. Magnetic hysteresis loops measured through *in situ* polar and longitudinal Kerr effects for growting Co films on a Pd(111) single crystal. The numbers indicate the thickness of Co films, t_{Co}.

~100 Oe. Above 5 ML, polar hysteresis loops start to change and show a hard axis loop, while the longitudinal ones become square in shape with small coercivities. It is clear from the *in-situ* SMOKE data that SRT takes place between 5 and 6 ML Co.

In order to better understand spin switching behavior during the reversal process, especially in the transition region, we have measured Kerr hysteresis loops of both *p*- and *s*-waves for two polar and one longitudinal configurations for $t_{Co} = 5$, 5.25, and 6 ML as demonstrated in Fig. 3. These data are necessary to determine 3D magnetization vector of the film during the magnetization reversal process. As described earlier, we used Eqs. (2), where each value of Θ_j^i can be obtained from the SMOKE data shown in Fig. 3, to determine three components, M_x, M_y, and M_z of the magnetization vector $\boldsymbol{M}$.

The resulting values of M_x, M_y, and M_z as a function of $\boldsymbol{H}$ are shown in Fig. 4, along with their parametric representation on the *xy*, *yz*, and *xz* planes in Fig. 5. For a 5 ML Co film, a simple magnetization reversal is obtained due to strong perpendicular magnetic anisotropy, as seen in Fig. 2. Magnetic fields above 90 Oe easily saturate magnetizations along the film normal direction, as demonstrated by scattered data points around $M_x = M_y = 0$ in the *xy* projection, around $M_z = 1$, $M_x = M_y = 0$ in the *xz* and *yz* planes.

For a 5.25 ML Co film, a complex reversal motion of magnetization is observed, which itself demonstrates the power of 3D vector magnetometry using SMOKE. Both M_x and M_y components are considerable except at high field, as seen in *xy* projection. At high fields the two components are near zero since the film is saturated in the perpendicular direction. As the applied field decreases, the two compo-

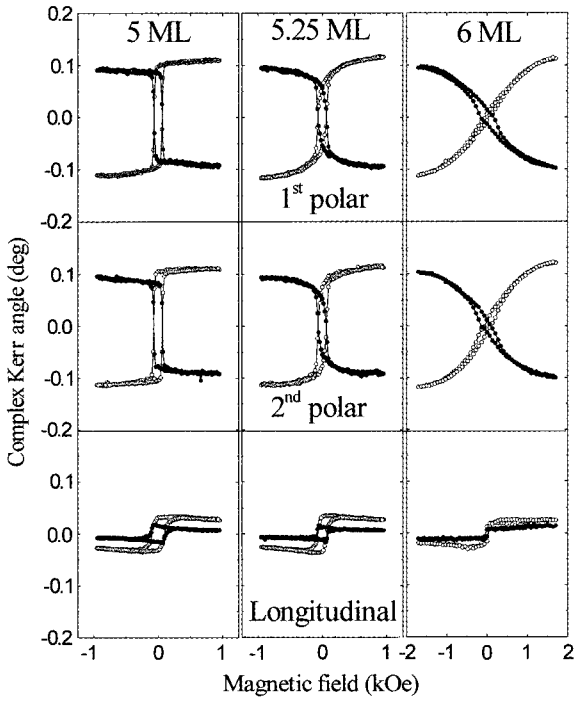

Fig. 3. SMOKE hysteresis loops measured with *p*- (open circles) and *s*- (solid circles) waves for t_{Co}=5, 5.25, and 6 ML. Each measurement configuration is described in Fig. 1.

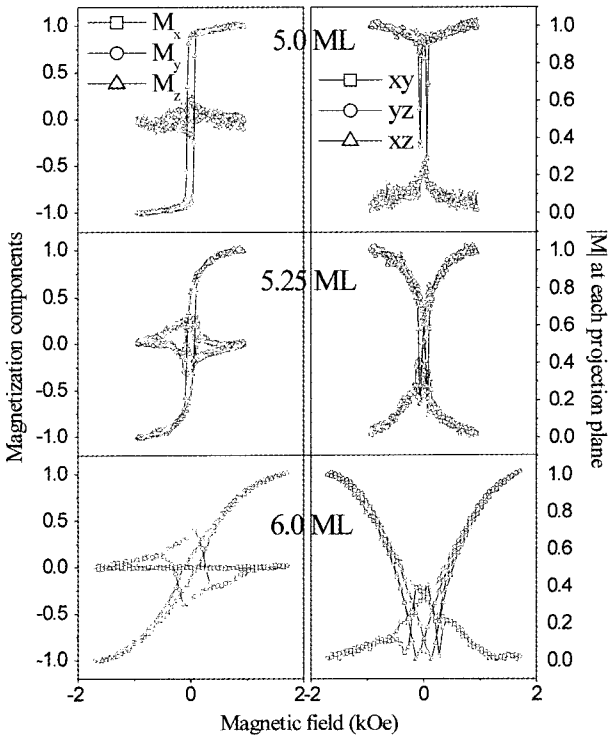

Fig. 4. Hysteresis loops of the M_x, M_y, and Mz components of $\boldsymbol{M}$ in left panel and the magnitude of $\boldsymbol{M}$ projected on the *xy*, *yz*, and *xz* planes in right panel for t_{Co}=5, 5.25, and 6 ML.

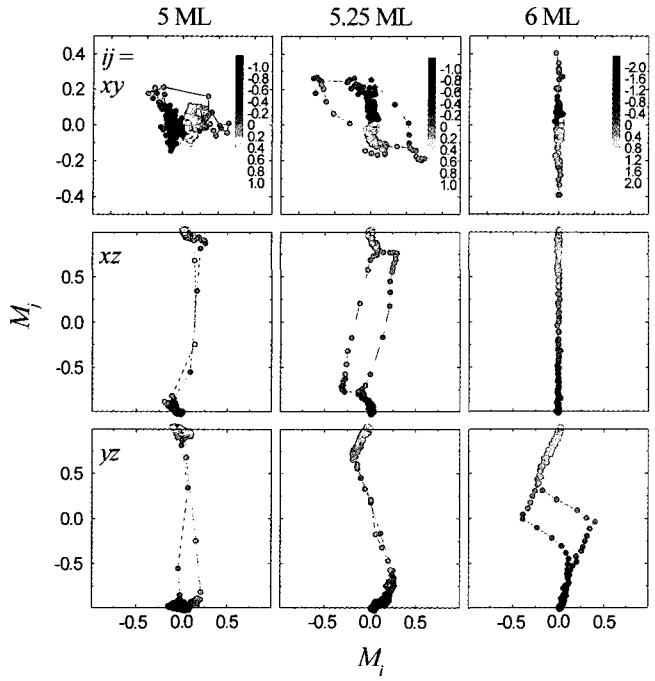

Fig. 5. 2D representations of $\boldsymbol{M}$ projected on the *xy*, *yz*, and *xz* planes which show 3D $\boldsymbol{M}$ reversal motions. Scale bars indicate the strength of magnetic field applied perpendicular to the film plane. This parametric representation of M is obtained from the data of M_x, M_y, and M_z shown in Fig. 4.

nents increase. The magnetization reversal process in *xz* plane is irreversible, but the *yz* projection shows reversible behavior in magnetic fields applied normal to the film.

In a 6 ML Co film, as seen in each plane, M_x is not observed at all, but M_y is observed at low fields along the film normal. In the *yz* plane, as the saturation field decreases, the M_z component decreases while M_y increases, indicating initial coherent rotation. Further decrease in the normal field forms multidomains of in-plane magnetization, and the remanance of M_y indicates an imbalance of areas of opposite directions of $\boldsymbol{M}$ along the *y*-axis. As the field increases in the negative *z*-direction, wall displacement of in-plane domains reduces the M_y component, and then coherent rotation of in-plane magnetization follows toward the perpendicular direction.

5. Summary

We have studied the spin-reorientation transition of ultrathin Co films grown on a Pd (111) single crystal using *in situ* SMOKE 3D vector magnetometry, which enables the determination of 3D magnetization vector during the reversal process. In the transition range of spin reorientation, each component of $\boldsymbol{M}$ shows different reversal behavior. For 5 ML Co with perpendicular magnetization, multidomains of perpendicular magnetization are formed and switch via collective spin rotation near a coercive field. For 6 ML Co with in-plane magnetization, coherent rotation of magnetization orientations occurs from perpendicular to in-plane as the saturation field decreases, and then multidomains of in-plane magnetization are formed near the coercive field. For the case of 5.25 ML, where a canted magnetization phase is observed, in-plane components of $\boldsymbol{M}$ rotate in the plane at a low field during the reversal process. As demonstrated in this work, this technique is very useful to better understand magnetization reversal processes with the aid of 3D vector representation of $\boldsymbol{M}$.

Acknowledgements

This work was supported by the Korean Ministry of Science and Technology through the Creative Research Initiatives Program.

References

[1] R. Allenspach, J. Magn. Magn. Mater., **129**, 160 (1994).
[2] J. Thomassen, F. May, B. Feldmann, M. Wutting, and H. Ibach, Phys. Rev. Lett., **69**, 3831 (1992).
[3] Y. T. Millev, H. P. Oepen, and J. Kirschner, Phys. Rev., B **57**, 5848 (1998).
[4] E. R. Moog and S. D. Bader, Superlattice and Microstructure **1**, 543 (1985); S. D. Bader, J. Magn. Magn. Mater., **100**, 440 (1991).
[5] B. Heinrich and J. F. Cochran, Adv. Phys., **42**, 523 (1993); S. Hope, E. Gu, B. Choi, and J. A. C. Bland, Phys. Rev. Lett., **80**, 1750 (1998).
[6] Z. Q. Qui, J. Pearson, and S. D. Bader, Phys. Rev. Lett., **67**, 1646 (1991); Y. Li and K. Baberschke, Phys. Rev. Lett., **68**, 1208 (1992).
[7] Z. Q. Qiu, J. Pearson, and S. D. Bader, Phys. Rev. Lett., **70**, 1006 (1993).
[8] A. Berger, A. W. Pang, and H. Hopster, Phys. Rev., B **52**, 1078 (1995).
[9] M. Farle, B. Mirwald-Schulz, A. N. Anisimov, W. Platow, and K. Baberschke, Phys. Rev., B **55**, 3708 (1997).
[10] J.-W. Lee, J.-R. Jeong, D.-H. Kim, J. S. Ahn, J. Kim, and S.-C. Shin, Rev. Sci. Instrum., **71**, 3801 (2000).
[11] C.-Y. You and S.-C. Shin, Appl. Phys. Lett., **69**, 1315 (1996); J. Appl. Phys., **84**, 541 (1998).
[12] Sung-Chul Shin, Jeong-Won Lee, Sang-Koog Kim, and Jonggeol Kim, Appl. Phys. Lett., submitted (2000).
[13] R. Allenspach, M. Stampanoni, and A. Bishof, Phys. Rev. Lett., **65**, 3344 (1990); S. Padovani, I. Chado, F. Scheurer, and J. P. Bucher, Phys. Rev., B **59**, 11887 (1999).